INTERNATIONAL ATOMIC ENERGY AGENCY
UNITED NATIONS EDUCATIONAL, SCIENTIFIC AND CULTURAL ORGANIZATION
INTERNATIONAL CENTRE FOR THEORETICAL PHYSICS
I.C.T.P., P.O. BOX 586, 34100 TRIESTE, ITALY, CABLE: CENTRATOM TRIESTE

H4-SMR 471/12

COLLEGE ON MEDICAL PHYSICS

10 - 28 SEPTEMBER 1990

DIGITAL RADIOGRAPHY:

QUANTITATIVE ANALYSIS OF DIAGNOSTIC IMAGE INFORMATION (I) & (II)

Kunio Doi

Kurt Rossmann Laboratories for Radiologic Image Research
University of Chicago
Chicago
USA

Lectures presented at the College on Medical Physics,
International Center for Theoretical Physics,
Trieste, Italy
10-28 September 1990

Digital Radiography:
Quantitative Analysis of Diagnostic Image Information (I) and (II)

Kunio Doi, Ph.D.

Kurt Rossmann Laboratories for Radiologic Image Research
Department of Radiology, The University of Chicago
Chicago, Illinois 60637 USA

Abstract

A number of computerized schemes being developed for computer-aided diagnosis (CAD) are reviewed. In distinguishing between normal and abnormal lungs with interstitial infiltrates in chest images, the computerized classification method provided the ROC curve that is comparable to or superior to that obtained by an average radiologist. The computerized detection schemes indicated true-positive detection rate of approximately 70% for subtle lung nodules in chest radiographs and 90% for subtle clustered microcalcifications in mammograms, although several false positives were detected in each image. The automatically computed outlines of the heart shadows in chest radiographs were very similar to the contours traced by radiologists, and were used to obtain parameters related to the size and area of the projected heart. By using an iterative deconvolution technique, opacified vessels larger than 0.5 mm in DSA images were measured with an accuracy of approximately 0.1 mm. The vascular structures in angiograms were tracked accurately and automatically by using a double-square-box region-of-search method.

1. Introduction

One of the most useful aspects of digital radiography, and picture archiving and communication systems (PACS) is the utilization of quantitative image information for diagnosis. Quantitative analysis of digital radiographic images may provide a basis for detection and characterization of lesions. Thus, potential lesion sites may be identified to alert the radiologist's attention prior to or during his or her interpretation so that false negatives may be reduced. In addition, the objective data obtained from quantitative analysis of lesions may be used by radiologists to avoid or complement subjective judgments. This application of digital image data for diagnosis has been referred to generally as computer-aided diagnosis (CAD). In this paper, a number of computerized schemes (1-17) being developed for CAD are reviewed, and preliminary results obtained with clinical images including chest radiographs, mammograms and angiograms are presented.

2. Computerized analysis of chest radiographs

2.1 Detection and characterization of interstitial lung disease

Interstitial lung disease is a common clinical entity that constitutes approximately 20% of lung abnormalities seen in chest radiographs at the University of Chicago Medical Center. Evaluation of diffuse interstitial disease in chest radiographs is considered a difficult task in diagnostic radiology, however (18). This difficulty is due to (a) the numerous patterns and complex variations that are involved, (b) the lack of firmly established correlation between radiologic and pathologic findings, and (c) variations among radiologists in the terms that they use to describe the associated radiographic patterns, which are not defined objectively. This subjectivity could be reduced and the accuracy of radiologic interpretation potentially increased if quantitative computerized methods that provide an objective assessment of lung texture patterns can be developed.

In order to detect and characterize interstitial disease, an automated method (1,2)

is being developed for the determination of physical texture measures in digital chest radiographs. This method is based on an analysis of the power spectrum of lung texture. The overall scheme of the approach is illustrated in Fig. 1. First, approximately 20 square regions of interest (ROI's), each with a 64 x 64 (6.4 mm x 6.4 mm) matrix size, are sampled from inter-rib spaces (3). The fluctuating patterns of the lung texture are isolated by correcting for the nonuniform background trends caused by the gross anatomy of the lung and chest wall; these trends are estimated using a two-dimensional surface-fitting technique. The resulting power spectrum of the lung texture is subsequently filtered by the visual-system response of the human observer (4). Finally, the root-mean-square (RMS) variation and the first moment of the power spectrum are calculated to obtain as quantitative measures of the magnitude and coarseness (or fineness), respectively, of the lung texture.

Figure 2 illustrates chest images of one normal and three abnormal lungs with nodular, reticular and honeycomb patterns. The two texture measures obtained from these chest images are shown in Fig. 3. The ellipse in the lower right of this diagram indicates the expected range ($\pm$ one standard deviation) of texture measures for normal lungs. The texture measures obtained from the reticular pattern are generally scattered above those of the normal lung, indicating an increase in the RMS variation while the first moment of its power spectrum is comparable to that for the normal lung. The nodular pattern has a low-frequency content, and its RMS variation is comparable to or slightly greater than that of the normal lung. The honeycomb pattern has a large RMS variation and a low-frequency content. These results indicate clearly that these two texture measures can distinguish relatively obvious patterns in these abnormal lungs.

In order to create a database and to establish an automated classification scheme, texture measures were determined for 100 normal lungs and 100 abnormal lungs with various types of interstitial disease. The overall scheme of the approach for classification to distinguish between normal and abnormal lungs is described briefly

below (2). First, the two texture measures obtained from a given chest image are normalized by using the average and the standard deviation of texture measures for normal lungs in the database. A single texture index is derived from the two normalized texture measures in order to facilitate the computerized classification. Suspicious "abnormal ROIs" are identified initially as regions where the texture indices are above a preselected threshold value. The identified abnormal ROIs are then subjected to three independent tests to determine whether the chest image includes a grossly abnormal pattern, a mild localized abnormal pattern, and/or a mild diffuse abnormal pattern. A chest image containing any one of these abnormal patterns is considered abnormal.

In order to evaluate the usefulness of the automated classification scheme, this method was applied to the analysis of 60 chest images that included normal and abnormal lungs with mild interstitial disease, none of which was included in the database. In addition, an observer test was performed by six staff radiologists and six senior radiology residents. Figure 4 shows a comparison of ROC curves obtained by the 12 observers and by the automated classification method. It is apparent that the computerized approach can yield results comparable to or superior to those obtained by an average observer in distinguishing between normal and abnormal lungs with interstitial infiltrates. This encouraging result should be interpreted cautiously, however. It is unlikely that CAD techniques will be sufficiently versatile to replace radiologists in the foreseeable future; rather they will assist the radiologist by extracting objective and quantitative data from radiographic images. Implementation of computerized schemes such as this in digital radiography would provide radiologists with the option of using the computer program either as a second opinion or as a source of objective and quantitative data on digital radiographic images.

2.2 Automated detection of lung nodules

Detection and diagnosis of cancerous lung nodules in chest radiographs are among

the most important and difficult tasks performed by radiologists. It is well documented that radiologists' error rate (false-negative detection rate) of lung nodules is approximately 30%. Both Brett (19) and Nash et al. (20), who administered semiannual radiographic chest examinations, concluded that the prognosis for patients with lung cancer is improved by early radiographic detection. However, in a long-term project on lung cancer detection which was conducted at the Mayo Clinic, Muhm et al. (21) found that 90% of subsequently diagnosed peripheral lung carcinomas were visible, in retrospect, on earlier radiographs. The observer error which caused these lesions to be missed may be due to the camouflaging effect of the surrounding anatomic background on the nodule of interest, or to the subjective and varying decision criteria used by radiologists. Underreading of a radiograph may be due to a lack of clinical data, lack of experience, a premature discontinuation of a film reading because a definite finding is identified, focusing of attention on another abnormality by virtue of a specific clinical question, failure to review previous films, and/or distractions.

The characteristic features of lung nodules and the surrounding normal anatomic background are being investigated in order to develop a computer-vision algorithm for use as an aid in the detection of nodules in digital chest radiographs (5-7). A schematic diagram of the nodule detection scheme is shown in Fig. 5. The approach begins with an attempt, by means of a difference-image technique, to increase the conspicuity of nodules by eliminating the camouflaging background of the normal lung anatomy. This is accomplished by creating two processed images from a single digital chest image; one processed image enhances the nodule and the other suppresses the nodule, with the background kept essentially the same in the two processed images. It is expected, then, that the difference between the two processed images would consist primarily of the nodule superimposed on a relatively uniform backgrounds in which the detection task will be relatively straightforward. Feature extraction techniques, such as tests for circularity, size, and their variation with threshold level, are subsequently applied in

order to isolate suspected nodules.

The result of this computerized detection scheme is illustrated in Figs. 6 and 7. The chest image in Fig. 6 shows a large, low-contrast nodule which is overlapped by the cardiac shadow; the detection of this nodule may be considered difficult. Figure 7 shows the same image with the computer output represented by circles and the location of the nodule indicated by a "T" marker. The overlap of the circle with T indicates a true-positive detection; that is, the nodule is correctly detected by computer. Circles alone indicate false-positive detections; that is, locations suspected by the computer at which no nodule was present. Currently, the computerized detection scheme can achieve an average true-positive detection rate of approximately 70% for subtle lung nodules, which is comparable to that achieved by radiologists. However, the current algorithm may produce several false positives in each chest image as illustrated in Fig. 7. Most false positives are caused by a part of a rib, crossing points of ribs, pulmonary vessels or other artifacts. From the result of the observer study, radiologists seem capable of ignoring most of these obvious false positives. However, it will be important to reduce the level of false positives further in the computerized detection of lung nodules prior to implementing this scheme in clinical practice.

2.3 Automated measurement of projected heart size

Cardiac size is an important and useful diagnostic parameter in chest radiographs. Unsuspected abnormal enlargement of the heart (cardiomegaly) is often diagnosed first by radiologists during the interpretation of chest radiographs. The conventional method of assessing cardiac enlargement is measurement of the cardiothoracic ratio (CTR), which is the ratio of the transverse diameter of the cardiac shadow to the greatest transverse diameter of the thorax (22,23). Many investigators have reported the relationship between cardiac disease and heart size, and they have demonstrated the usefulness of the CTR and/or estimated cardiac size in clinical

applications. Fuster et al. (23) investigated the relationship between mortality and prognostic factors such as the CTR by following patients with idiopathic dilated cardiomyopathy for 6 to 20 years. They found that the larger the CTR, the greater the probability of early death. They also found that mortality was 86% in patients with a CTR of 55% or more, compared to 40% in patients with a CTR below 55%. In posterior-anterior (PA) chest radiographs, 50% is generally accepted as an upper limit for the CTR in normal individuals.

An automated method (8) is being developed for determining a number of parameters related to the size and shape of the heart and of the lungs in chest radiographs. In order to provide a starting point for estimating the true cardiac outline, four radiologists traced their best estimates of the entire contour of the heart, including the largely invisible inferior margin, on 11 radiographs. It should be noted that manual tracing is not needed for application of the technique after it was developed. The Fourier transforms of these contours were analyzed and the results were used as a guide to obtain a shift-variant cosine function which was used to predict the cardiac contour by fitting a limited number of detected heart boundary points. These points were obtained from analysis of edge gradients in two orthogonal directions. A simple observer study indicated that the contours of the heart shadows computed for 60 chest radiographs were generally acceptable to radiologists as estimates of the size and area of the projected heart. The rib cage and the edges of the diaphragm were also detected, and thus enabled the determination of the projected thoracic area. From these results, it is possible to calculate the cardiothoracic ratio and other parameters, such as the ratio of the projected heart area to the projected thoracic area.

Figure 8 shows a chest radiograph and computed contour (white line) of the heart shadow in comparison with contours traced by four radiologists (dashed dark lines). It appears that the computed contour agrees within the variation of the four traces. Figure 9 illustrates an example of the CRT display of a computerized analysis which provides

the computed heart contour and the computed rib-cage edge superimposed on the chest image. The calculated parameters displayed on the right side include the cardiac transverse diameter, the cardiac height, the long and the broad diameters of the heart, the thoracic transverse diameter and the thoracic height as well as the CTR.

3. Computerized analysis of mammograms for automated detection of microcalcifications

Breast cancer is a leading cause of death in women. However, early diagnosis and treatment significantly improves the chance of survival for patients with breast cancer. X-ray mammography is the only diagnostic procedure with a proven capability for detecting early-stage, clinically occult breast cancers (24). Between 30% and 50% of breast carcinomas detected radiographically demonstrate microcalcifications on mammograms, and between 60% and 80% of breast carcinomas reveal microcalcifications upon microscopic examination. Therefore, any increase in the detection of microcalcifications by mammography should lead to further improvement in its efficacy for the detection of early breast cancer.

The application of computer-based methods is being investigated to the detection of microcalcifications in digital mammograms (9-12). The computer detection system is based on a difference-image technique in which a signal-suppressed image is subtracted from a signal-enhanced image to suppress the structured background in the mammogram. Locally adaptive grey-level thresholding and region-growing techniques are then used to isolate potential microcalcifications from the remaining noise background. Signal-extraction tests based on the physical characteristics of microcalcifications, such as the size, contrast, frequency content and the clustering of microcalcifications, are subsequently employed to distinguish true signals from noise and artifacts. The computer output indicates potential clusters of microcalcifications by circles superimposed on a mammogram, as shown in Fig. 10. The performance of this

automated detection scheme when it was applied to 60 normal and abnormal mammograms with subtle microcalcifications is shown in Fig. 11. The present computer method can achieve a true-positive cluster detection rate of approximately 90% at a false-positive detection rate of 4 clusters per image. The potential usefulness of such a computer-aided system for mammographic interpretation is demonstrated by radiologists' improved detection accuracy of microcalcifications in clinical mammograms, as illustrated by the ROC curves in Fig. 12. Comparison of the two ROC curves indicates that radiologists' detection of clustered microcalcifications was significantly improved (p 0.01) when the computer output was displayed on the mammograms.

4. Computerized analysis of vascular images

4.1 Automated measurement of vessel size

Accurate measurement of vessel sizes for quantitative analysis of stenotic lesions is of great value in the assessment of progression or regression of vascular disease (25). The severity of stenotic lesions traditionally has been assessed by visual interpretation of angiograms in terms of percent stenosis. However, several studies have documented a large intra- and inter-observer variability in the subjective visual evaluation of stenosis. In order to reduce the uncertainty caused by the subjective judgment of vessel narrowing and to provide a good estimate of the severity of stenoses, many investigators have devised methods for the quantitative analysis of digital arteriograms.

An iterative deconvolution technique is being developed to determine the size of a "blurred" vessel in a digital subtraction angiographic (DSA) image by taking into account the unsharpness of the DSA system (13,14). Initially, a region of interest in a contrast-filled vessel is selected in a DSA image, and the center line of the opacified vessel is determined by fitting the locations of the peak pixel values along the vessel image with a polynomial curve. The blurred image profile is then obtained from pixel values across the vessel in a direction perpendicular to the vessel center line. The iterative

deconvolution technique is then applied to this blurred image profile. A schematic diagram of this technique is shown in Fig. 13. With this technique, the vessel-image profile is compared iteratively with profiles calculated for various size vessels, which are obtained from a cylindrical vessel model and from the known line spread function of the DSA system, until a profile is found for which the root-mean-square (RMS) difference is minimized. The size of the cylindrical vessel yielding the matched profile is considered the best estimate of the unknown vessel size. Studies with a blood vessel phantom indicated that vessels larger than 0.5 mm could be measured with an accuracy and precision of approximately 0.1 mm, as shown in Fig. 14, which is about 1/3 of the pixel size in our DSA system. In order to apply this technique to coronary arteriograms, methods are being developed for estimating the background in the vicinity of the vessels, so as to obtain an accurate vessel profile. Figure 15 shows an example of computerized analysis of a stenotic lesion in a coronary arteriogram.

4.2 Automated tracking of vascular images

Angiograms can provide useful morphologic and functional information concerning the vascular system for the diagnosis of vascular diseases. However, in conventional angiography, this information is not fully utilized because diagnoses are based primarily upon a qualitative interpretation of the angiograms. In digital angiographic systems, on the other hand, accurate quantitative data can be obtained by computerized image processing. However, all analyses of the vascular system require the identification either of specific portions of the vascular tree or of the entire vascular tree. Therefore, one of the most basic and important elements of quantitative analysis is the computerized, automated tracking of the vessels in the vascular tree. Once the vascular tree has been tracked, additional analyses can proceed automatically to obtain quantitative information about the vessels, which may include detection of stenosis or aneurysm, quantitation of their severity, three-dimensional representation of the

vascular tree, or blood-flow analysis of multiple vessel segments.

A double-square-box region-of-search algorithm (15-17) is being developed by which the connected vessels in the entire vascular tree are tracked accurately and automatically. The local diameters and contrasts of the vessels being tracked are determined accurately by the iterative deconvolution technique. At each tracking point, the vessel size information is employed to establish square-box regions of search for identification of subsequent tracking points. Both the vessel size and the vessel contrast are monitored to determine the point at which tracking of a particular vessel will be terminated. The vessel sizes, contrasts and centerline positions along the vascular tree can be used subsequently for additional quantitative analyses of the vessels. At present, the algorithm accurately tracks the vascular tree into regions in which the ratio between the vessel contrast and the RMS noise is approximately 3 for vessel sizes of 0.5 mm or more. Figures 16 and 17 compare a DSA image and a computer-generated image, which was reproduced from the vessel information obtained by tracking. It is apparent that the computer-generated image is very similar to the original DSA image, even for small and low-contrast vessels. This result indicates the level of the accuracy of the vessel information derived from our tracking technique.

5. Conclusion

The initial results obtained from computerized analysis of digital radiographic images are encouraging, and appear to indicate the potential usefulness of computer-aided diagnostic schemes in assisting radiologists' diagnosis. However, development of computer-aided schemes is still at an early stage. It will be necessary, therefore, to fully understand the basic image features of normal and abnormal patterns in radiographic images, to establish databases for specific applications, and to devise specific approaches for varied problems in radiographic examinations.

References

1. Katsuragawa S, Doi K, MacMahon H: Image feature analysis and computer-aided diagnosis in digital radiography: Detection and characterization of interstitial lung disease in digital chest radiographs. Med Phys. 15: 311-319, 1988.

2. Katsuragawa S, Doi K, MacMahon H: Image feature analysis and computer-aided diagnosis in digital radiography: Classification of normal and abnormal lungs with interstitial disease in chest images. Med. Phys. 16: 38-44, 1989.

3. Powell GF, Doi K, Katsuragawa S: Localization of inter-rib spaces for lung texture analysis and computer-aided diagnosis in digital chest images. Med. Phys. 15: 581-587, 1988.

4. Katsuragawa S, Doi K, MacMahon H: Quantitative analysis of lung texture for computer-aided diagnosis of interstitial disease in digital chest radiographs. Proc. SPIE 914: 371-374, 1988.

5. Giger ML, Doi K, MacMahon H: Image feature analysis and computer-aided diagnosis in digital radiography. 3. Automated detection of nodules in peripheral lung fields. Med. Phys. 15: 158-166, 1988.

6. Giger ML, Doi K, MacMahon H: Computerized detection of lung nodules in digital chest radiographs. Proc. SPIE 767: 384-386, 1987.

7. Giger ML, Doi K, MacMahon H, Yin F-F: Image-processing techniques used in the computer-aided detection of radiographic lesions in anatomic background. Proc. SPIE 914: 635-637, 1988.

8. Nakamori N, Doi K, Sabeti V, MacMahon H: Image feature analysis and computer-aided diagnosis in digital radiography: Automated analysis of sizes of heart and lung in digital chest images. Med. Phys. 17: 342-350, 1990.

9. Chan HP, Doi K, Galhotra S, Vyborny CJ, MacMahon H, Jokich PM: Image feature analysis and computer-aided diagnosis in digital radiography. 1. Automated detection of microcalcifications in mammography. Med Phys. 14: 538-548, 1987.

10. Chan HP, Doi K, Vyborny CJ, Metz CE, MacMahon H, Jokich P, Galhotra S: Digital mammography: Development of a computer-aided system for detection of microcalcifications. Proc. SPIE 767: 367-370, 1987.

11. Chan HP, Doi K, Vyborny CJ, Lam KL, Schmidt RA: Computer-aided detection of microcalcifications in mammograms: Methodology and preliminary clinical study. Investigative Radiology 23: 664-671, 1988.

12. Chan HP, Doi K, Lam KL, Vyborny CJ, Schmidt RA, Metz CE: Digital characterization of clinical mammographic microcalcifications: Applications in computer-aided detection. Proc. SPIE 914: 591-593, 1988.

13. Fujita H, Doi K, Fencil LE, Chua KG: Image feature analysis and computer-aided diagnosis in digital radiography. 2. Computerized determination of vessel sizes in digital subtraction angiography. Med. Phys. 14: 549-556, 1987.

14. Fencil L, Doi K, Hoffmann K: Accurate analysis of blood vessel sizes and stenotic lesions by use of stereoscopic DSA systems. Investigative Radiology 23: 33-41, 1988.

15. Hoffmann KR, Doi K, Chan HP, Fencil L, Fujita H, Muraki A: Automated tracking of the vascular tree in DSA images using a double-square-box region-of-search algorithm. Proc. SPIE 626: 326-333, 1986.

16. Hoffmann KR, Doi K, Chan HP, Chua KG: Computer reproduction of the vasculature using an automated tracking method. Proc. SPIE 767: 449-453, 1987.

17. Hoffmann KR, Doi K, Chan HP, Takamiya M: Three-dimensional reproduction of coronary vascular trees using the double-square-box method of tracking. Proc. SPIE 914: 375-378, 1988.

18. Fraser RG, Pace JA: Diagnosis of diseases of the chest (Saunders, Philadelphia, 1970), pp. 423-434.

19. Brett GZ: Earlier diagnosis and survival in lung cancer. Br. Med. J. 4: 260, 1969.

20. Nash FA, Morgan JM, Tomkins JG: South London lung cancer study. Br. Med. J. 2: 715, 1968.

21. Muhm JR, Miller WE, Fontana RS, Sanderson DR, Uklenhopp MA: Lung cancer detected during a screening program using four-month chest radiographs. Radiology 148: 609, 1983.

22. Sutton D: A Textbook of Radiology and Imaging, (Churchill Livingston), 4th edition, vol. 1; pp. 554-556, 1987.

23. Fuster V. Gersh BJ, Giuliani ER, Tajik AJ, Brandenburg RO, Frye RL: The natural history of idiopathic dilated cardiomyopathy. Am. J. Cardiol. 47: 525-531, 1981.

24. Seidman H, Gelb SK, Silverburg E, LaVerda N, Lubera JA: Survival experience in the Breast Cancer Detection Demonstration Project. CA Cancer J Clin 37: 258, 1987.

25. Gould KL: Quantitation of coronary artery stenosis in vivo. Circulation Research 57: 341-353, 1987.

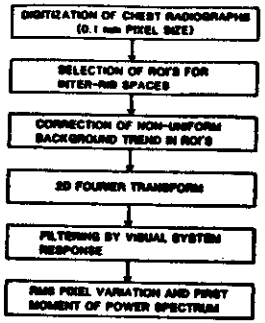

Fig. 1 Overall scheme for quantitative analysis of lung textures in chest radiographs.

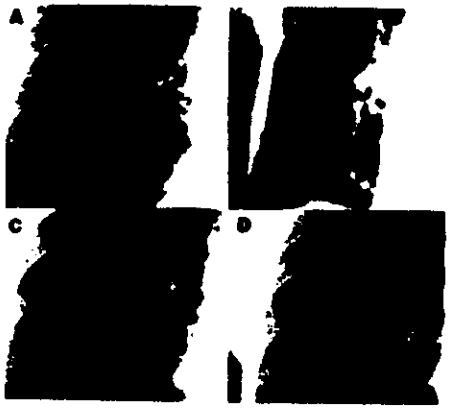

Fig. 2 Chest images of one normal (D) and three abnormal lungs with nodular (C), reticular (B) and honeycomb (A) patterns.

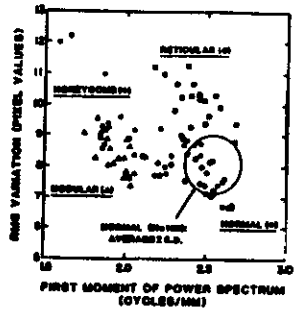

Fig. 3 Texture measures obtained from many ROIs selected in inter-rib spaces of the four lungs shown in Fig. 2.

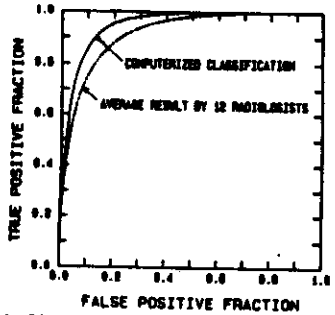

Fig. 4 ROC curves obtained by 12 radiologists and automated classification method in detecting abnormal lungs with interstitial infiltrates.

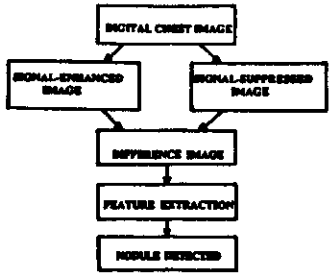

Fig. 5 Schematic diagram of the automated nodule detection scheme.

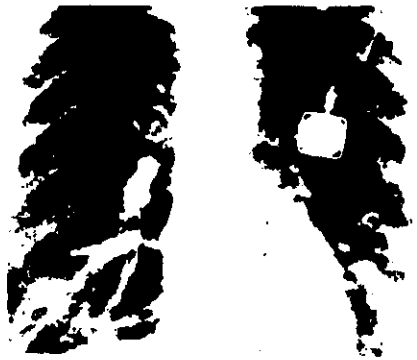

Fig. 6 A chest image with a large, low-contrast nodule overlapped by the cardiac shadow.

Fig. 7 Illustration of the computer output (circles) indicating potential sites of lung nodules.

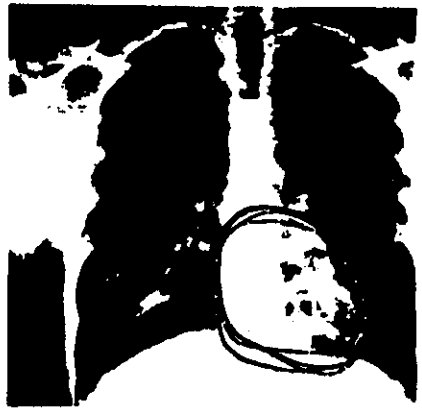

Fig. 8 Comparison of the computed contour (white line) of the heart shadow with contours traced by four radiologists (dashed dark lines).

Fig. 9 Illustration of the CRT display of a computerized analysis of the heart shadow in a chest image.

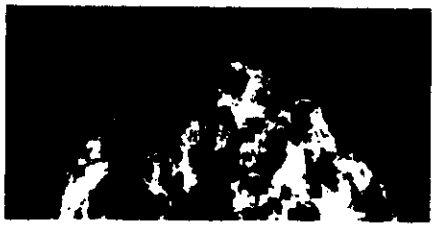

Fig. 10 Illustration of the computer output (circles) indicating potential sites of clustered microcalcifications in a mammogram. A circle located at the upper right indicates a true-positive detection, and other circles false-positive detections.

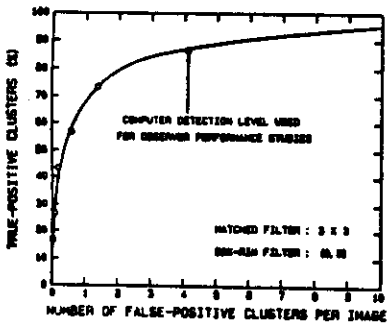

Fig. 11 Performance of the automated detection scheme obtained from 60 mammograms.

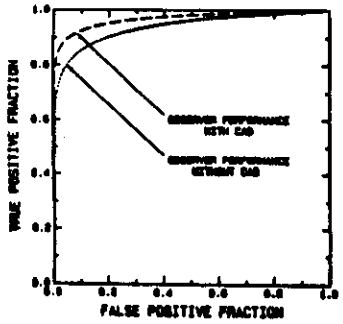

Fig. 12 Comparison of ROC curves obtained by radiologists with and without the computer-aid in detecting clustered microcalcifications in mammograms.

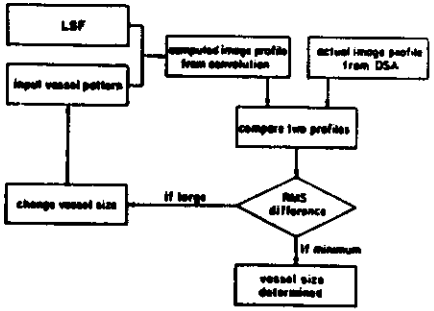

Fig. 13 Schematic diagram of an iterative deconvolution technique in determining the size of an opacified vessel image in DSA.

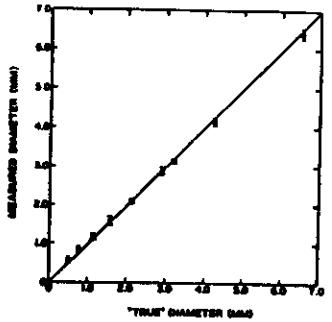

Fig. 14 Comparison of measured sizes obtained with the iterative deconvolution technique and "true" sizes of vessel phantoms.

Fig. 15 Illustration of the CRT display of a computerised analysis of a stenotic lesion in coronary arteriogram.

Fig. 16. A DSA image of external cranial arteries.

Fig. 17 A computer-generated image obtained from tracking the DSA image in Fig. 16 by using the double-square-box region-of-search technique.